Published in final edited form as:
Photochem Photobiol. 2014 July ; 90(4): 889–895. doi:10.1111/php.12270.

Enhanced Efficacy of Photodynamic Therapy via a Sequential Targeting Protocol

David Kessel[1,*] and **John J. Reiners Jr**[1,2]

[1]Department of Pharmacology, Wayne State University, Detroit, MI 48201

[2]Institute of Environmental Health Sciences, Wayne State University, Detroit, MI 48201

Abstract

This study was designed to examine determinants of the discovery that low-dose lysosomal photodamage (lyso-PDT) could potentiate the efficacy of subsequent low-dose mitochondrial photodamage (mito-PDT). The chlorin NPe6 and the benzoporphyrin BPD were used to separately target lysosomes and mitochondria, respectively, in murine hepatoma cells. Lyso-PDT (LD_5 conditions) followed by mito-PDT (LD_{15} conditions) enhanced the loss of the mitochondrial membrane potential, activation of procaspases-3/7 and photokilling. Reversing the sequence was less effective. The optimal sequence did not enhance reactive oxygen species formation above that obtained with low-dose mito-PDT. In contrast, alkalinization of lysosomes with bafilomycin also enhanced low-dose mito-PDT photokilling, but via a different pathway. This involves redistribution of iron from lysosomes to mitochondria leading to enhanced hydroxyl radical formation, effects not observed after the sequential procedure. Moreover, Ru360, an inhibitor of mitochondrial calcium and iron uptake, partially suppressed the ability of Bafilomycin to enhance mito-PDT photokilling without affecting the enhanced efficacy of the sequential protocol. We conclude that sequential PDT protocol promotes PDT efficacy by a process not involving iron translocation, but via promotion of the pro-apoptotic signal that derives from mitochondrial photodamage.

INTRODUCTION

Use of photosensitizing agents to sensitize neoplastic tissues to light is termed photodynamic therapy (PDT) (1,2). While PDT is generally defined as a therapeutic clinical measure, in the context of this report, the term will be used to indicate a photodynamic process involving cells in culture. Since the reactive oxygen species (ROS) formed during PDT have a very short biologic half-life, photodamage is confined to regions where photosensitizing agents localize. This phenomenon makes it possible to direct photodamage to specific sub-cellular loci if photosensitizing agents have a sufficiently precise localization pattern.

Several photosensitizers, including Pc 4 (3,4), preferentially localize to mitochondria. PDT-induced mitochondrial photodamage (mito-PDT) results in destruction of mitochondria-

*Corresponding author: dhkessel@med.wayne.edu.

associated Bcl-2 (5,6), loss of mitochondrial membrane potential ($\Delta\Psi_m$), release of cytochrome c into the cytosol and subsequent initiation of apoptosis (7,8). Photokilling of cultured tumor cells by Pc 4 was recently reported to be enhanced by pretreatment with Bafilomycin (Baf) or chloroquine (9,10), agents that promote the alkylinization of lysosomes. Although both agents block steps in the development of an autophagic response following PDT, potentially negating the prosurvival properties of autophagy, their ability to potentiate mito-PDT was attributed to a different mechanism. This involved translocation of lysosomal iron to mitochondria where Fe^{++} could promote hydroxyl radical ($^{\bullet}OH$) formation via Fenton chemistry (9,10).

The chlorin photosensitizer N-aspartyl chlorin e6 (NPe6) localizes primarily to acidic organelles such as late endosomes and lysosomes (11,12). Lysosomal PDT (lyso-PDT) with NPe6 has multiple effects depending upon sensitizer concentration and light dose. In the case of the murine hepatoma 1c1c7 cell line, high-dose PDT results in a very rapid and virtually simultaneous alkalinization and permeabilization of the lysosomes (11). Release of lysosomal cathepsins into the cytoplasm can subsequently cleave the pro-apoptotic protein BID to tBID (11,13), resulting in permeabilization of mitochondria and the release of cytochrome c (14). With milder PDT conditions (~LD_{30}) the alkylinization of lysosomes is slower and is followed by a later release of lysosomal cathepsins. At still lower PDT doses (~LD_{10}), neither alkalinization nor permeabilization of lysosomes could be detected, but such conditions are sufficient to disrupt endocytosis (15).

In this study, we examined phenomena associated with sequential low-dose PDT involving the mitochondrial photosensitizer benzoporphyrin derivative termed BPD (7), and the lysosomal sensitizer NPe6. Effects were compared to results obtained with BPD-PDT alone and in combination with Bafilomycin. Results obtained indicate that we have defined two independent mechanisms for the perturbation of lysosomes, either of which can potentiate the efficacy of subsequent mitochondrial photodamage.

MATERIALS AND METHODS

Chemicals and supplies

NPe6 was provided by Dr. Kevin M. Smith, Louisiana State University. BPD (benzoporphyrin derivative, Verteporfin) was purchased from VWR (Cat No 1711461). Other reagents were obtained from Sigma-Aldrich and were of the highest available purity. Fluorescent probes were provided by Life Technologies, Inc.. Diethyl-3-3′-(9,10-anthracenediyl)bis acrylate (DADB) was prepared and utilized as previously reported (16). Synthesis of the fluorescent probe RhoNox-1 (RN-1) was carried out as described in reference 17. RN-1 is a non fluorescent N-oxide of Rhodamine B that is converted to a fluorescent product upon contact with Fe^{++}.

Cell culture and clonogenic assays

Growth of murine hepatoma 1c1c7 cells and procedures for clonogenic assays have been described (18).

PDT protocols

Cultures were grown on cover slips in 30 mm diameter plastic dishes. These were incubated with 0.5 μM BPD, 40 μM NPe6 or both for 1 h at 37°C. In some studies Ru360 (10 μM) and/or Baf (50 nM) were also added at the time of addition of photosensitizer. After 1 h the medium was replaced and the dishes were irradiated using a 600-watt quartz-halogen source filtered through 10 cm of water to remove wavelengths of light > 900 nm. The bandwidth of the light beam was further confined by interference filters (Oriel, Stratford CT) to 660 ± 10 nm for NPe6 or 690 ± 10 nm for BPD. Irradiation times were calculated based on clonogenic studies, so as to yield the desired effects on viability.

Microscopy protocols

Singlet oxygen and hydroxyl radical formation were monitored with the probes DADB and APF, respectively (16,19,20). The fluorescence of DADB is quenched in the presence of singlet oxygen, while APF is converted to a fluorescent product upon interaction with hydroxyl radical. DADB (10 μM) and APF (2.5 μM) were added to cultures at the time of photosensitizer addition. Changes in DADB and APF fluorescence were monitored directly after irradiation using 405 nm excitation and 525 nm emission, and 490 nm excitation and 515 nm emission, respectively. Photodamage to mitochondria resulting in loss of membrane potential ($\Delta\Psi_m$) was assessed using MitoTracker Orange (MTO) or MitoTracker Green (MTG), as previously described (21,22).

To track intracellular localization of ferrous ion, cultures were treated with RN-1 (2.5 μM) for 60 min, during the photosensitizer loading incubation. Fluorescence was monitored using 510–560 nm excitation and 570 nm emission. Mitochondria or lysosomes and RN-1 could be simultaneously imaged using MTG or LTG. These probes (2 μM) were loaded during 10 min incubations at 37° directly after irradiation. Fluorescence emission of MTG and LTG (510 nm) is well separated from RN-1 (570 nm). A 650 nm low-pass filter was inserted into the emission pathway to eliminate long-wavelength fluorescence from NPe6 and BPD,

To test for the possibility that lysosomal photodamage might cause relocalization of BPD, cells were treated with both BPD and NPe6. Sites of BPD localization were identified by fluorescence microscope (excitation = 400 nm, emission = 680–700 nm). Insertion of a 690 ± 10 nm bandpass filter into the emission beam prevented 660 nm NPe6 fluorescence from reaching the CCD camera. We then irradiated the sample on the microscope stage (660 nm 75 mJ/cm sq). BPD localization was then assessed in a separate image. Using MetaMorph software, the first and second images were overlaid using false colors (red, green). Pixels showing red or green would then identify lack of coincidence; yellow = coincidence.

Phase-contrast and fluorescence images were acquired with a Nikon E-600 microscope using a Rolera EM-CCD camera. MetaMorph software (Molecular Devices, Sunnyvale CA) was used to examine the relative pixel intensities of images. Images were thresholded to select appropriate regions, and pixel brightness ± SD was determined using the ‘region statistics’ program as previously described (16).

DEVDase assays

Cells were collected 1 hr after irradiation and assayed for DEVDase activity (12). A kit provided by Invitrogen was used for this purpose (cat. no. E13184). Enzyme levels are reported in terms of nmol product/min/mg protein. Each assay was performed in triplicate. The Micro Lowry assay was used to estimate protein concentrations, using bovine serum albumin as the standard.

Statistical analysis

Analysis of data was carried out using the independent groups t-test. We indicate where differences in values were statistically different ($p < 0.05$) from untreated controls, or other specified data.

RESULTS AND DISCUSSION

The utilization of sequential PDT protocols requires that the absorption spectra of the photosensitizers are sufficiently different so that light used to activate one sensitizer has no effect on the other. This is true for NPe6 (660 nm) and BPD (690 nm). Both have sufficiently narrow bandwidth so there is minimal overlap (Fig. 1).

Light-dose studies were utilized to identify irradiation conditions with NPe6 and BPD alone that reproducibly represented ~LD_5 and ~LD_{15} conditions, respectively (as defined by clonogenic assays). There are hereafter referred to as low-dose NPe6 or low-dose BPD PDT. Sequential low-dose PDT with the two photosensitizers resulted in an enhanced inhibition of colony formation. Optimal suppression of colony formation, however, occurred when low-dose NPe6 PDT preceded low-dose BPD PDT (Table 1).

Phase contrast microscopy studies were consistent with an apoptotic outcome following sequential PDT (not shown). DEVDase activity is commonly used to monitor the activities of caspase-3 and -7, the major executioner proteases associated with apoptosis. Low-dose NPe6 or BPD photodamage alone had only slight effects on DEVDase specific activities (Table 2), while the sequential protocol resulted in DEVDase activities that exceeded simple additive effects. As anticipated from the absorption spectra of the photosensitizers, irradiation at 660 nm had no demonstrable effect on cells photosensitized with BPD. In agreement with the colony formation assays, optimal enhancement of DEVDase activities occurred when low-dose NPe6 PDT preceded low-dose BPD PDT (Table 2).

The major reactive oxygen species (ROS) generated upon irradiation of NPe6 or BPD is singlet oxygen (19,23). DADB has been established as a reliable probe for this ROS species: fluorescence is lost upon interaction with $^1O_2$ (16). Low-dose NPe6-PDT alone had no significant effect on DADB fluorescence (Fig. 2A vs C, E) whereas, low-dose BPD-PDT caused a demonstrable loss of probe fluorescence (Fig. 2A vs B). This effect was not enhanced by prior low-dose NPe6 PDT (Fig. 2B vs D, E). Hence, enhanced killing as a result of the sequential PDT protocol was not associated with increased singlet oxygen production.

Mitochondrial photodamage commonly leads to a loss of the mitochondrial membrane potential ($\Delta\Psi_m$). Studies involving MTO, a fluorescent probe used tor monitor $\Delta\Psi_m$, indicated that low-dose BPD PDT alone caused a loss of $\Delta\Psi_m$ within 10 min of irradiation (Fig. 3A vs B). Low-dose NPe6 PDT did not, however, alter $\Delta\Psi_m$ (Fig. 3A vs C). The sequential PDT protocol potentiated the loss of $\Delta\Psi_m$ only when lysosomal photodamage came first (Fig. 3B vs D and E). The presence of Ru360 (10 μM) did not alter any of these results (Fig. 3, panels F–J).

Bafilomycin B_1 is a potent inhibitor of the vacuolar proton pump that maintains the acidity of lysosomes (24,25). A consequence of Baf exposure is the release of Fe^{2+} from lysosomes (9,10,26). Recent studies reported that Baf pretreatment significantly enhanced the killing of cultured cells by the mitochondrial photosensitizer Pc 4 [9,10]. This effect was attributed to translocation of lysosomal iron stores to mitochondria, where Fenton chemistry could mediate formation of $^{\bullet}OH$. Exposure of 1c1c7 cultures to Baf for 60 min had no significant effect on 1c1c7 colony formation (Table 3), but markedly enhanced the cytotoxicity of low-dose BPD PDT (Table 3). To determine whether this effect involved iron translocation, we carried out colocalization analyses of cells loaded with RN-1, a molecule that fluoresces red upon interaction with ferrous iron (17), and fluorescent green probes that preferably localize to mitochondria (MTG) or lysosomes (LTG). In untreated cultures, virtually every lysosome showed a strong colocalization of RN-1 and LTG, as indicated by bright fluorescent yellow puncta (Fig. 4F). In contrast, very few mitochondria showed colocalization of RN-1 and MTG (Fig. 4A). However, after Baf treatment a considerable percentage of cells showed colocalization of MTG and RN-1 (Fig. 4B), indicating accumulation of Fe^{++} in mitochondria.

Ru360 inhibits mitochondrial import of both Ca^{++} and Fe^{++} (27). Exposure of cultures to Ru360 alone had no significant effect on colony formation (Table 3), but Ru360 did partially suppress the phototoxicity of Baf + low-dose BPD PDT (Table 3). These data are therefore consistent with previous reports indicating that Baf can potentiate cell killing by subsequent mito-PDT via a mechanism involving iron accumulation in mitochondria (9,10).

The sequential PDT protocol (lysosomal photodamage first) did not mimic the effect of Baf. Colocalization analyses revealed no detectable translocation of Fe^{++} to mitochondria (Fig. 4A vs C) following low-dose NPe6 PDT. Moreover, when low-dose NPe6-PDT preceded low-dose BPD-PDT, there was neither a detectable loss of lysosomal Fe^{++} (Fig. 4H) nor an accumulation of mitochondrial Fe^{++} (Fig. 4D). Since the images shown in Fig. 4 were captured within minutes of irradiation, we considered the possibility that iron leakage from lysosomes might be delayed after NPe6 PDT. There was, however, no evidence of mitochondrial Fe^{2+} accumulation 60 min after low-dose NPe6 PDT alone (Fig. 5A), or following sequential low-dose NPe6 and BPD PDT (Fig. 5B). Furthermore, treatment with Ru360 offered no protection against BPD, NPe6/BPD, or BPD/NPe6 PDT induced loss of $\Delta\Psi_m$ (Fig. 3B vs G, D vs I, and E vs J, respectively), or colony formation (Table 1).

Hydrogen peroxide is generated as a secondary ROS species in Type II PDT reactions (28). In the presence of Fe^{++} it can participate in Fenton chemistry to generate $^{\bullet}OH$. We assessed the formation of $^{\bullet}OH$ with APF, a probe that fluoresces upon interaction with $^{\bullet}OH$, and to a

much lesser extent with singlet oxygen (19,20,29). Very little fluorescence was observed in untreated cultures (Fig. 6A), in cultures treated for 60 minutes with BAF (Fig. 6B), or after low-dose NPe6 PDT (Fig. 6D). Intracellular APF fluorescence did increase after low-dose BPD-induced photodamage (Fig. 6C,G). Prior low-dose NPe6-PDT did not significantly enhance APF fluorescence (Fig. 6E,G). In contrast, supplementation of the medium with BAF prior to low-dose BPD PDT significantly increased both APF fluorescence (Fig. 6F,G) and photokilling (Table 3).

Data shown in Figure 6 indicate that pretreatment with BAF, but not prior low-dose lyso-PDT, potentiated the generation of •OH by low-dose BPD PDT. Since BAF induces translocation of Fe^{++} to mitochondria, and BPD localizes in mitochondria, it is reasonable to speculate that the increased APF fluorescence occurs in mitochondria.. Additional colocalization studies would be required to identify the site(s) of the APF fluorescence.

Fig. 7 demonstrates the lack of an effect of lysosomal photodamage on BPD localization. Cells were loaded with BPD and NPe6 as described in the legend to Fig. 2. An image of BPD fluorescence was then acquired using 400 nm excitation and acquiring fluorescence at 680–720 nm. This eliminates the 660 nm fluorescence from NPe6. The cells were then irradiated on the microscope stage (660 nm, 75 mJ.sq cm) and another image of the same field acquired.

CONCLUSIONS

This study examined two different procedures in which lysosomal perturbation potentiated the efficacy of subsequent mitochondrial photodamage. One of these utilized the vacuolar ATPase inhibitor Baf and entailed lysosomal alkalinization and the release of lysosomal iron. Baf-induced potentiation of BPD PDT-induced photokilling was partially suppressed by Ru360, and was correlated with increased APF fluorescence, reflecting more •OH formation. These effects presumably derive from translocation of lysosomal-derived Fe^{2+} to mitochondria leading to added •OH formation via iron-catalyzed Fenton chemistry. Our results with BPD are in agreement with recent studies involving Baf and another mitochondrial photosensitizer, the phthalocyanine Pc 4 (9,10).

The ability of BAF to potentiate the toxicity of mitochondrial damage is not unique to PDT. Lemasters' laboratory reported that Baf can also sensitize hepatocytes to killing by the non-PDT oxidative stressor tert-butylhydroperoxide (26). This potentiation was also a consequence of translocation of lysosomal Fe^{++} to mitochondria and enhanced ROS generation.

The procedure for lysosomal perturbation used here involved a low PDT dose mediated by NPe6 that did not alter the localization of BPD. It is known that a lethal level of photodamage involving NPe6 will cause a rapid and irreversible alkalinization and permeabilization of lysosomes in 1c1c7 cells (11,30). Conditions used in the current study (~LD_5), however, caused neither lysosome alkalinization nor the translocation of lysosomal ferrous iron. Nevertheless, low-dose NPe6 PDT did potentiate BPD phototoxicity. This effect was not suppressed by Ru360 nor was it accompanied by increased •OH formation.

These differences clearly distinguish the mechanisms whereby low-dose NPe6 PDT and BAF potentiate photokilling by subsequent low-dose mitochondrial photodamage.

It is not clear whether the 60 min incubation with 40 μM NPe6 was sufficient for the photosensitizer to reach every lysosome via endocytosis, perhaps missing some with a higher iron content. In a previous study using a 66 μM level of NPe6 for only 30 min, we were able to achieve a good coincidence between NPe6 and Lysotracker Blue fluorescence localization patterns (11). This suggests that we are likely reaching a significant number of lysosomes, regardless of their position in the endocytotic process.

The mechanism by which low-dose NPe6 PDT potentiates mitochondrial PDT is not yet clear. We know that low-dose NPe6 PDT can influence physiological processes that are distal to endosomes/lysosomes, e.g., suppression of endocytosis of the plasma membrane (15,31). Furthermore, PDT directed against endosomes and lysosomes also impairs pathways involving mTOR (32). This effect may play a role in the promotion of BPD efficacy by prior lysosomal photodamage. Other roles for mTOR in PDT responses have been proposed (33). Based on data shown in Table 2, we propose that the NPe6 – BPD sequence of irradiation results in amplification of a pro-apoptotic signal elicited by mitochondrial photodamage, leading to a promotion of photokilling..

Acknowledgments

This study was supported by grant CA23378 from the National Cancer Institute, National Institutes of Health. We thank Ann Marie Santiago for excellent technical assistance.

References

1. Dougherty TJ, Gomer CJ, Henderson BW, Jori G, Kessel D, Korbelik M, Moan J, Peng Q. Photodynamic therapy. J Natl Cancer Inst. 1998; 90:889–905. [PubMed: 9637138]
2. Agostinis P, Berg K, Cengel KA, Foster TH, Girotti AW, Gollnick SO, Hahn SM, Hamblin MR, Juzeniene A, Kessel D, Korbelik M, Moan J, Mroz P, Nowis D, Piette J, Wilson BC, Golan J. Photodynamic therapy of cancer: an update. CA Cancer J Clin. 2011; 61:250–281. [PubMed: 21617154]
3. Trivedi NS. Quantitative analysis of Pc 4 localization in mouse lymphoma (LY-R) cells via double-label confocal fluorescence microscopy. Photochem Photobiol. 2000; 71:634–639. [PubMed: 10818795]
4. Lam M, Oleinick NL, Nieminen AL. Photodynamic therapy-induced apoptosis in epidermoid carcinoma cells. Reactive oxygen species and mitochondrial inner membrane permeabilization. J Biol Chem. 2001; 276:47379–47386. [PubMed: 11579101]
5. Kessel D, Reiners JJ Jr. Apoptosis and autophagy after mitochondrial or endoplasmic reticulum photodamage. Photochem Photobiol. 2007; 83:1024–1028. [PubMed: 17880495]
6. Usuda J, Azizuddin K, Chiu SM, Oleinick NL. Association between the photodynamic loss of Bcl-2 and the sensitivity to apoptosis caused by phthalocyanine photodynamic therapy. Photochem Photobiol. 2003; 78:1–8. [PubMed: 12929741]
7. Peng TI, Chang CJ, Guo MJ, Wang YH, Yu JS, Wu HY, Jou MJ. Mitochondrion-targeted photosensitizer enhances the photodynamic effect-induced mitochondrial dysfunction and apoptosis. Ann N Y Acad Sci. 2005; 1042:419–428. [PubMed: 15965088]
8. Kessel D, Oleinick NL. Photodynamic therapy and cell death pathways. Methods Mol Biol. 2010; 635:35–46. [PubMed: 20552338]

9. Saggu S, Hung HI, Quiogue G, Lemasters JJ, Nieminen AL. Lysosomal signaling enhances mitochondria-mediated photodynamic therapy in A431 cancer cells: role of iron. Photochem Photobiol. 2012; 88:461–468. [PubMed: 22220628]
10. Hung HI, Schwartz JM, Maldonado EN, Lemasters JJ, Nieminen AL. Mitoferrin-2-dependent Mitochondrial Iron Uptake Sensitizes Human Head and Neck Squamous Carcinoma Cells to Photodynamic Therapy. J Biol Chem. 2013; 288:677–686. [PubMed: 23135267]
11. Reiners JJ Jr, Caruso JA, Mathieu P, Chelladurai B, Yin XM, Kessel D. Release of cytochrome c and activation of pro-caspase-9 following lysosomal photodamage involves Bid cleavage. Cell Death Differ. 2002; 9:934–944. [PubMed: 12181744]
12. Reiners JJ Jr, Kleinman M, Kessel D, Mathieu PA, Caruso JA. Nonesterified cholesterol content of lysosomes modulates susceptibility to oxidant-induced permeabilization. Free Radic Biol Med. 2012; 50:281–294. [PubMed: 21074609]
13. Stoka V, Turk B, Schendel SL, Kim T-H, Cirman T, Snipas SJ, Ellerby LM, Bredesen D, Freeze H, Abrahamson M, Brommer D, Krajewski S, Reed JC, Yin X-M, Turk V, Salvesen GS. Lysosomal protease pathways to apoptosis: cleavage of Bid, not pro-caspases, is the most likely route. J Biol Chem. 2001; 276:3149–3157. [PubMed: 11073962]
14. Korsmeyer SJ, Wei MC, Saito M, Weiler S, Oh KJ, Schlesinger PH. Proapoptotic cascade activated by BID, which oligomerizes BAK or BAX into pores that result in the release of cytochrome c. Cell Death Differ. 2000; 7:1166–1173. [PubMed: 11175253]
15. Kessel D, Price M, Caruso J, Reiners JJ Jr. Effects of photodynamic therapy on the endocytic pathway. Photchem Photobiol Sci. 2011; 10:491–498.
16. Kessel D, Price M. Evaluation of diethyl-3-3′-(9,10-anthracenediyl)bis acrylate as a probe for singlet oxygen formation during photodynamic therapy. Photochem Photobiol. 2012; 88:717–720. [PubMed: 22296586]
17. Hirayama T, Kensuke O, Nagasawa H. A highly selective turn-on fluorescent probe for iron(II) to visualize labile iron in living cells. Chem Sci. 2013; 4:1250–1256.
18. Andrzejak M, Price M, Kessel D. Apoptotic and autophagic responses to photodynamic therapy in 1c1c7 murine hepatoma cells. Autophagy. 2011; 7:979–984. [PubMed: 21555918]
19. Price M, Reiners JJ, Santiago AM, Kessel D. Monitoring singlet oxygen and hydroxyl radical formation with fluorescent probes during photodynamic therapy. Photochem Photobiol. 2009; 85:1177–1181. [PubMed: 19508643]
20. Kessel D, Reiners JJ Jr. Light-Activated Pharmaceuticals: Mechanisms and Detection. Isr J Chem. 2012; 52:674–680. [PubMed: 23990688]
21. Kessel D, Caruso JA, Reiners JJ Jr. Potentiation of photodynamic therapy by ursodeoxycholic acid. Cancer Res. 2000; 60:6985–6988. [PubMed: 11156400]
22. Kessel D, Luo Y, Mathieu P, Reiners JJ Jr. Determinants of the apoptotic response to lysosomal photodamage. Photochem Photobiol. 2000; 71:196–200. [PubMed: 10687394]
23. Price M, Heilbrun L, Kessel D. Effects of the oxygenation level on formation of different reactive oxygen species during photodynamic therapy. Photochem Photobiol. 2013; 89:683–686. [PubMed: 23216021]
24. Bowman EJ, Siebers A, Altendorf K. Bafilomycins: A class of inhibitors of membrane ATPases from microorganisms, animal cells, and plant cells. Proc Natl Acad Sci USA. 1988; 85:7972–7976. [PubMed: 2973058]
25. Gagliardi S, Rees M, Farina C. Chemistry and structure activity relationships of bafiomycin A1, a potent and selective inhibitor of the vacuolar H+-ATPase. Curr Med Chem. 1999; 6:1197–1212. [PubMed: 10519916]
26. Uchiyama A, Kim J-S, Kon K, Jaeschke H, Ikejima K, Watanabe S, Lemaster JJ. Translocation of iron from lysosomes into mitochondria is a key event during oxidative stress-induced hepatocellular injury. Hepatology. 2008; 48:1644–1654. [PubMed: 18846543]
27. Ying WL, Emerson J, Clarke MJ, Sanadi DR. Inhibition of mitochondrial calcium ion transport by an oxo-bridged dinuclear ruthenium ammine complex. Biochemistry. 1991; 30:4949–4952. [PubMed: 2036363]
28. Price M, Terlecky SR, Kessel D. A role for hydrogen peroxide in the pro-apoptotic effects of photodynamic therapy. Photochem Photobiol. 2009; 85:1491–1496. [PubMed: 19659920]

29. Setsukinai K, Urano Y, Kakinuma K, Majima HJ, Nagano T. Development of novel fluorescence probes that can reliably detect reactive oxygen species and distinguish specific species. J Biol Chem. 2003; 278:3170–3175. [PubMed: 12419811]

30. Caruso JA, Mathieu PA, Joiakim A, Leeson B, Kessel D, Sloane BF, Reiners JJ Jr. Differential susceptibilities of murine hepatoma 1c1c7 and Tao cells to the lysosomal photosensitizer NPe6: Influence of aryl hydrocarbon receptor on lysosomal fragility and protease contents. Mol Pharmacol. 2004; 65:1016–1028. [PubMed: 15044632]

31. Kessel D. Inhibition of endocytic processes by photodynamic therapy. Lasers Surg Med. 2011; 43:542–547. [PubMed: 22057481]

32. Weyergang A, Berg K, Kaalhus O, Peng Q, Selbo PK. Photodynamic therapy targets the mTOR signaling network in vitro and in vivo. Mol Pharmaceut. 2009; 6:255–264.

33. Dewaele M, Martinet W, Rubio N, Verfaillie T, de Witte PA, Piette J, Agostinis P. Autophagy pathways activated in response to PDT contribute to cell resistance against ROS damage. J Cell Mol Med. 2011; 15:1402–1414. [PubMed: 20626525]

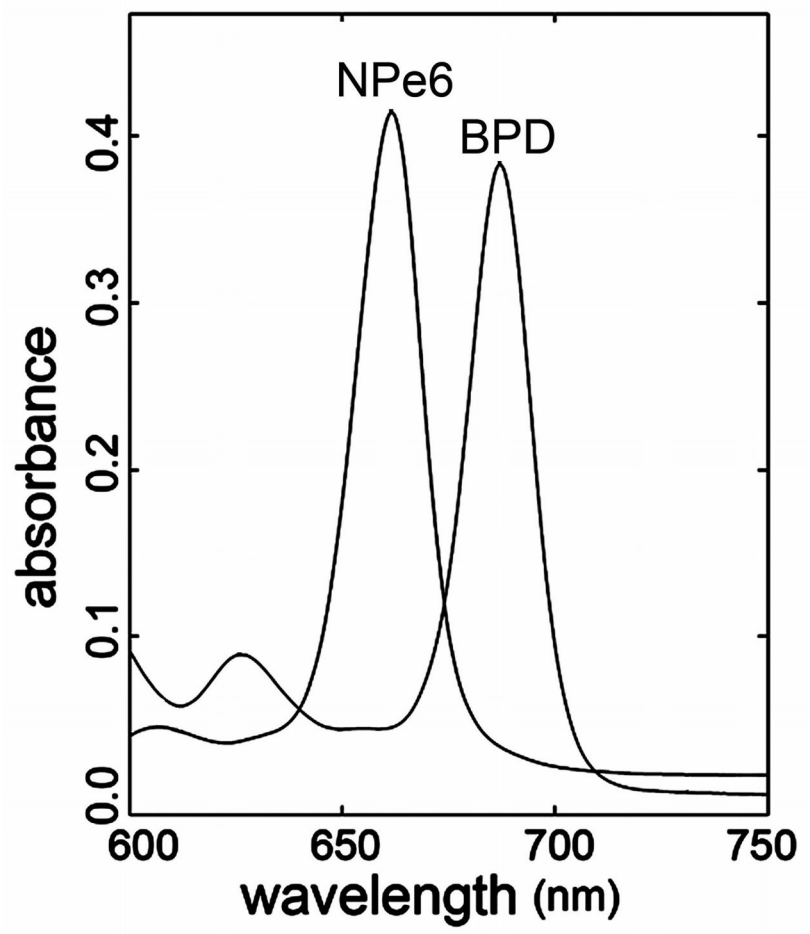

Figure 1.
Excitation spectra of NPe6 and BPD (10 μM) in ethanol.

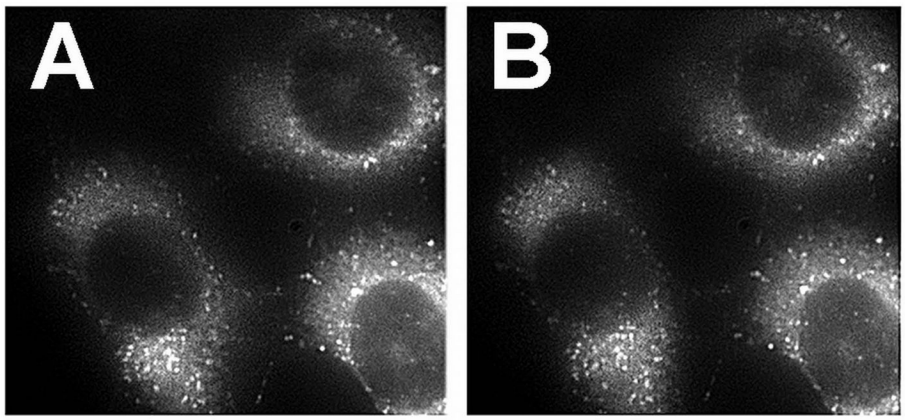

Figure 2.

Cells were treated with NPe6 and BPD (see legend to Fig. 1), and an image of BPD fluorescence acquired (EM = 400 nm, EX = 680–700 nm). After irradiation on the microscope stage (660 nm, 75 mJ/cm sq), a second image of the same field was was acquired. Magnification = 1000 x.

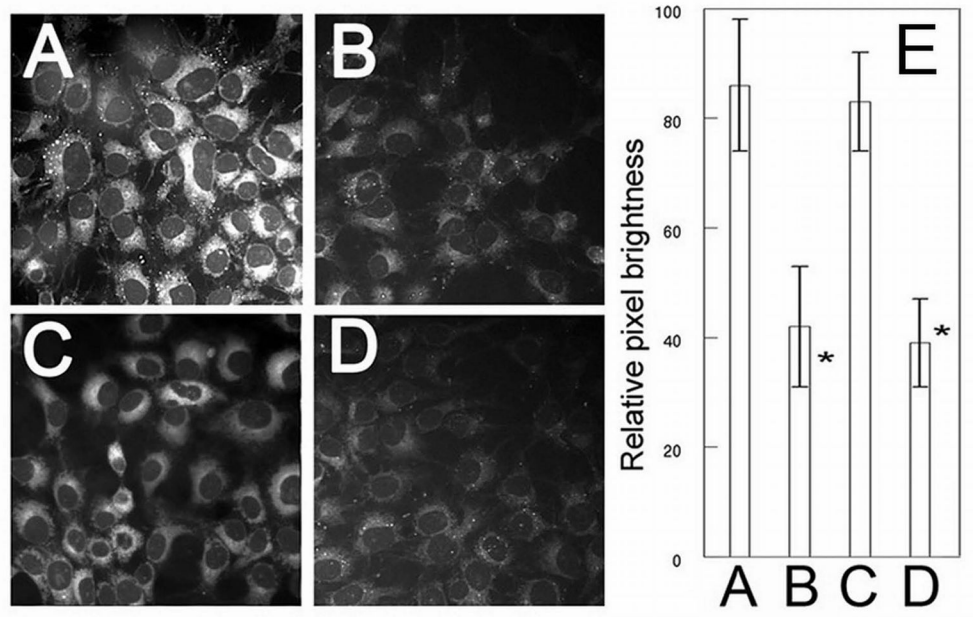

Figure 3.

Singlet oxygen production following irradiation. Cultures were incubated with DADB (10 μM) + 0.5 μM BPD or 40 μM NPe6 for 60 min, and then refed with fresh medium and irradiated at 690 nm (BPD, 37.5 mJ/sq cm), or at 660 nm (NPe6, 75 mJ/sq cm), or sequentially at both wavelengths. Additional cultures were incubated with only DADB. Images of DADB fluorescence were captured in (A) untreated control cultures, or directly after: (B) low-dose BPD PDT, (C) low-dose NPe6 PDT, (D) sequential NPe6-BPD PDT. Panel (E) shows pixel brightness analyses of ~100 cells per field. Note that DADB fluorescence is lost upon interaction with singlet oxygen. *Significantly less than either A or C ($p<0.05$). There was no significant difference between A and C, or B and D.

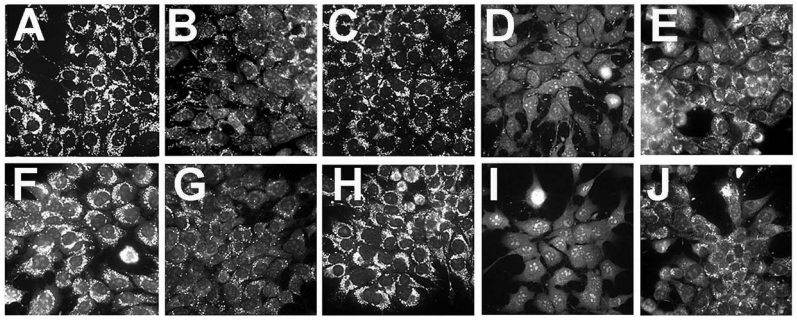

Figure 4.

Effects of PDT on maintenance of the mitochondrial membrane potential. Panels A–E: cultures were loaded with NPe6 and BPD and irradiated as described in Fig. 2. Panels F–J: cultures treated with Ru360 (10 μM) during photosensitization and after washing and refeeding with fresh medium. MTO (2 μM) was added immediately after irradiation and imaging was carried out 10 minutes later. A,F = untreated control cells, B, G = irradiation at 690 nm (37.5 mJ/cm sq), C,H = irradiation at 660 nm (75 mJ/sq cm), D, I = irradiation at 660 nm before 690 nm, E,J = irradiation at 690 nm before 660 nm.

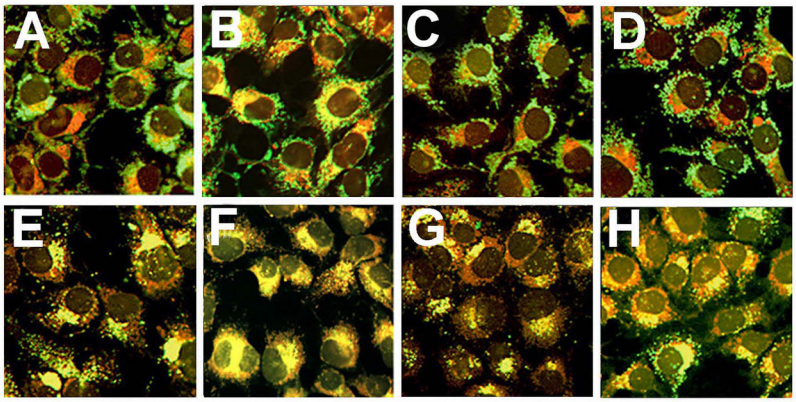

Figure 5.

Fluorescence co-localization of iron and mitochondrial or lysosomal loci shortly after irradiation. Cultures were loaded with sensitizers and irradiated as described in Fig. 2. RN1 (red fluorescence) or Baf was added to cultures 1 h prior to irradiation. The mitochondrial fluorescence probe MTG (A–D, green) or the lysosomal fluorescence probe LTG (E–H, green) were added directly after irradiation, and imaged 10 min later. Treatments were: (A,E) no treatment; (B,F) in the presence of Baf; (C,G) after NPe6-PDT; and (D,H) after NPe6-PDT followed by BPD-PDT.

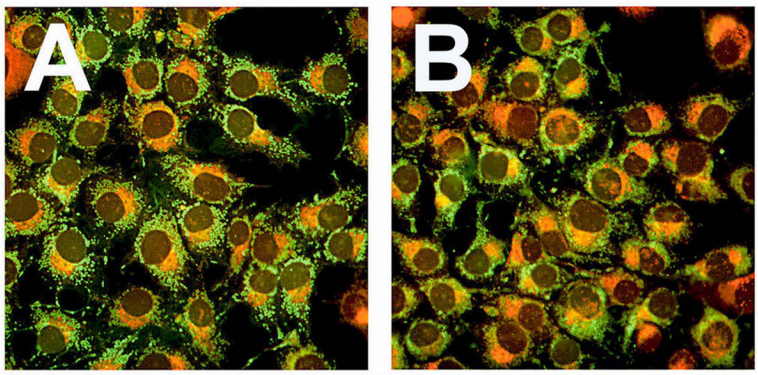

Figure 6.

Fluorescence co-localization analyses of iron and mitochondrial loci 60 min after irradiation. Cultures were incubated with RN1 and NPe6 ± BPD, washed, refed, and irradiated as in Fig. 4. Fluorescence co-localization of RN-1 (red) and MTG (green) was performed as described in Figure 4 except that images were captured 60 after irradiation. Treatments were: (A) low-dose NPe6 PDT; (B) low-dose NPe6 PDT followed by low-dose BPD PDT.

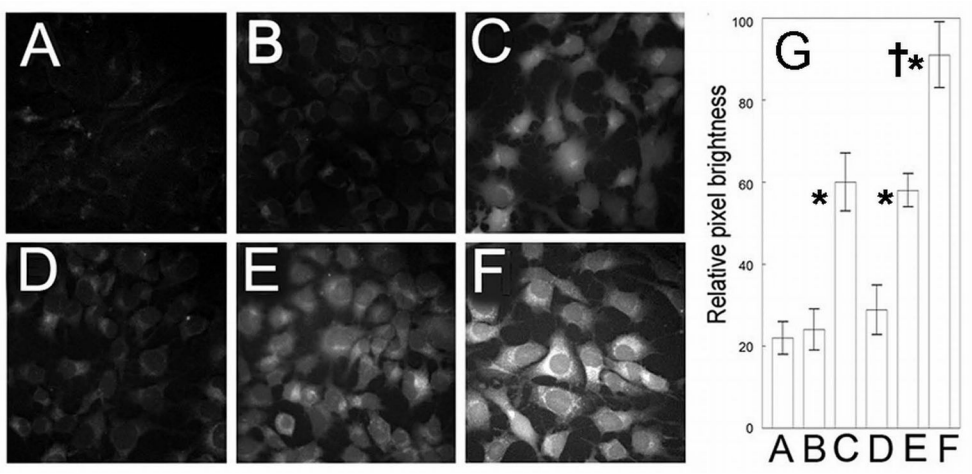

Figure 7.

Effects of Bafilomycin on PDT-induced hydroxyl radical formation. Cultures were incubated for 60 min with 2.5 μM APF and (as specified) 50 μM Baf, 0.5 μM BPD, or 40 μM NPe6 before being washed and refed. Treatments were: (A) untreated control, (B) Baf alone, (C) low-dose BPD PDT, (D) low-dose NPe6 PDT, (E) NPe6 PDT → BPD PDT, (F) Baf → BPD PDT. Panel (G) shows the pixel brightness analyses of 100 cells per treatment. *Significantly greater fluorescence than in untreated controls, BAF alone, and low dose NPe6 PDT, $p<0.05$. †Significantly greater than all other treatment groups, $p< 0.05$.

Table 1

Colony formation as a function of the PDT protocol; effects of Ru360

Conditions	Clonogenicity (%)	
	Additions	
	none	Ru360
No additions	100 ± 3	98 ± 4
BPD	83 ± 5	84 ± 3
NPe6	95 ± 2	92 ± 3
NPe6 ⇒ BPD	17 ± 3*†	15 ± 4*†
BPD ⇒ NPe6	58 ± 4*	53 ± 5*

For experimental conditions see the legend to Table 1. Ru360 (10 μM) was present where indicated. Data represent average ± SD for triplicate determinations.

*Statistically different from controls;

†statistically different from result obtained with reverse order of irradiation ($p < 0.05$).

Table 2

DEVDase activation as a function the PDT protocol

PDT	irradiation	DEVDase
Control	none	0.08 ± 0.01
BPD	690	0.22 ± 0.06
BPD	660	0.09 ± 0.02
NPe6	690	0.08 ± 0.01
NPe6	660	0.09 ± 0.02
BPD + NPe6	660 ⇒ 690	2.3 ± 0.11*†
BPD + NPe6	690 ⇒ 660	0.69 ± 0.07*

Cells were treated with 0.5 μM BPD and/or 40 μM NPe6 for 60 min, then resuspended in fresh medium and irradiated (660 nm @ 90 mJ/sq cm; 690 nm @ 37.5 mJ/sq cm). DEVDase activity was measured 60 min later and is expressed as nmol/mg protein/min. The sequence of irradiation wavelengths is shown in column 2. Data represent average ± SD for 3 separate experiments.

*Statistically different from controls;

†statistically different from result obtained with reverse order of irradiation ($p < 0.05$).

Table 3

Bafilomycin effects on photokilling by BPD PDT

Conditions	Clonogenicity (%)
No additions	100 ± 4
Bafilomycin	96 ± 5
Ru360	91 ± 4
BPD PDT	85 ± 6
Baf + BPD PDT	19 ± 3*
Ru360 + Baf + BPD PDT	46 ± 3*†

Conditions are specified in the legend to Table 1. Bafilomycin B_1 (Baf, 50 nM) or Ru360 (10 μM) were present during the 60 min BPD loading incubation. Cultures were then resuspended in fresh medium, irradiated and colony formation evaluated. Data represent average ± SD for triplicate samples.

* Statistically different from controls;

† statistically different from result obtained with reverse order of irradiation ($p < 0.05$). .